Journal of Magnetic Resonance 206 (2010) 59–67

Contents lists available at ScienceDirect

Journal of Magnetic Resonance

journal homepage: www.elsevier.com/locate/jmr

Evaluating the accuracy and precision of a two-compartment Kärger model using Monte Carlo simulations

M. Nilsson [a,*], E. Alerstam [b], R. Wirestam [a], F. Ståhlberg [a,c], S. Brockstedt [d], J. Lätt [e]

[a] Department of Medical Radiation Physics, Lund University, Lund, Sweden
[b] Department of Physics, Lund University, Lund, Sweden
[c] Department of Diagnostic Radiology, Lund University, Lund, Sweden
[d] Radiation Physics, Skåne University Hospital, Lund, Sweden
[e] MR Department, Center for Medical Imaging and Physiology, Skåne University Hospital, Lund, Sweden

ARTICLE INFO

Article history:
Received 3 March 2010
Revised 27 May 2010
Available online 9 June 2010

Keywords:
DW-MRI
Diffusion
Microstructure
Monte Carlo simulations
Diffusion time

ABSTRACT

Specific parameters of the neuronal tissue microstructure, such as axonal diameters, membrane permeability and intracellular water fractions are assessable using diffusion MRI. These parameters are commonly estimated using analytical models, which may introduce bias in the estimated parameters due to the approximations made when deriving the models. As an alternative to using analytical models, a database of signal curves generated by fast Monte Carlo simulations can be employed. Simulated diffusion MRI measurements were generated and evaluated using the two-compartment Kärger model as well as the simulation model based on a database containing signal curves from approximately 60 000 simulations performed with different combinations of microstructural parameters. A protocol based on a pulsed gradient spin echo sequence with diffusion times of 30 and 60 ms and with gradient amplitudes obtainable with a clinical MRI scanner was employed for the investigations. When using the analytical model, a major negative bias (up to approximately 25%) in the estimated intracellular volume fraction was observed for short exchange times, while almost no bias was seen for the simulation model. In general, the simulation model improved the accuracy of the estimated parameters as compared to the analytical model, except for the exchange time parameter.

© 2010 Elsevier Inc. All rights reserved.

1. Introduction

Specific characteristics of neuronal tissue microstructure can be assessed using diffusion magnetic resonance imaging (MRI), useful for investigating disease and development of cerebral matter. Examples of such characteristics are axonal or cell diameters, cell membrane permeability and intracellular water volume fractions. Axonal diameters have been estimated using nuclear magnetic resonance (NMR) spectrometers in excised neuronal tissue [1–3]. Using clinical MRI scanners, microstructural features of phantoms have been assessed [4] and recent studies suggest that this is feasible also *in vivo* [5–8].

Experiments aiming at the investigation of tissue microstructure are commonly designed to measure the diffusion-weighted (DW) signal intensity for different degrees of diffusion encoding (b-values) and different diffusion times (T_D), thereby probing the microstructure at different length and time scales [9]. Measurements designed to selectively probe the microstructure of white matter fibres are commonly performed in a single direction perpendicular to the fibre structure [1–5], although models have been developed to also estimate the fibre direction from diffusion measurements in multiple directions [6]. The analytical models employed to estimate the microstructural features comprise the DW signal from different intra- and extracellular components. However, it is challenging to accurately model the signal curves from these individual components, due to, for instance, long diffusion encoding durations, exchange between components and different relaxation rates for different components.

The modelling challenges are met by various assumptions, first regarding the tissue geometry and subsequently about the measurements on the geometry. For example, the tissue structure is commonly assumed to be comprised of ideal geometries, such as parallel planes, cylinders or spheres. For these ideal geometries, analytical models describing the signal curves have been derived under the assumption that the measurement produces a Gaussian phase distribution or that the diffusion encoding duration is infinitesimal [5,6,10–12]. For a tissue model based on one intracellular and one extracellular compartment, Monte Carlo simulations have been employed to investigate the validity of these measurement models. Meier et al. showed that it is possible to extract the intracellular exchange time under appropriate experimental conditions

* Corresponding author.
E-mail address: markus.nilsson@med.lu.se (M. Nilsson).

1090-7807/$ - see front matter © 2010 Elsevier Inc. All rights reserved.
doi:10.1016/j.jmr.2010.06.002

[13]. Nilsson et al. confirmed this, but found that the estimated intracellular volume fraction may be biased in case of short exchange times [5]. These studies suggest that a given measurement protocol yields accurate and precise results only for certain combinations of microstructural parameters. Alexander showed that under experimental conditions obtainable using a clinical MRI scanner, axonal diameters larger than approximately 5 μm are possible to estimate accurately in a two-compartment system, using an analytical model without exchange [6]. However, in the presence of compartmental exchange, the accuracy and precision of the estimated parameters has not been established and requires further investigation.

As an alternative to using analytical measurement models, microstructural parameters may be extracted using a database of signal curves obtained by using Monte Carlo simulations, similar to the approach by van Enden et al. [14]. Signal curves in the database can be considered as "fingerprints" of the microstructure and measured signal curves can be matched against these. This approach, herein denoted the simulation model, requires less assumptions regarding the measurement model than the analytical models, but relies on fast simulations in order to build a sufficiently large database without inordinate demands on computation times.

The aim of this study was to investigate the accuracy and the precision when estimating microstructural parameters in a two-compartment system with exchange, using simulated diffusion MRI data. The microstructural parameters were estimated from signal curves simulated for experimental settings and noise levels obtainable with a clinical MRI scanner. The performance in estimating the microstructural parameters was compared between two different measurement models, i.e. the analytical two-compartment Kärger model and the simulation model.

2. Theory

In DW magnetic resonance experiments, pulsed magnetic-field gradients cause a signal attenuation by producing a phase dispersion of the diffusing spins. The DW signal S is given by

$$S = \int_{-\infty}^{\infty} \cos(\phi) f(\phi) d\phi \tag{1}$$

where ϕ is the spin phase and $f(\phi)$ is the probability density of spin phases in a given volume and its Monte Carlo approximation S^* is obtained according to

$$S^* = \frac{1}{n} \sum_{k=1}^{n} \cos(\phi_k), \phi_k \in F(\phi) \tag{2}$$

where n is the number of particles. The phase ϕ_k is drawn from the distribution $F(\phi)$ using simulations, according to

$$\phi_k = \gamma \int_{t=0}^{T} \mathbf{r}_k(t) \cdot \mathbf{g}(t) dt \tag{3}$$

where γ is the gyromagnetic ratio, T is the time at which the MR signal is acquired and $\mathbf{g}(t)$ is the magnetic-field gradient [15]. The particle trajectory, $\mathbf{r}_k(t)$, is simulated as a random walk in a simulation geometry, defined by the tissue model and described by tissue parameters $\mathbf{m}$. In the two-compartment model employed in the present study, $\mathbf{m} = \{d, \tau_i, D_i, D_e, c_i\}$, where d is the cell diameter, τ_i is the intracellular exchange time, D_i and D_e are the physical intra- and extracellular diffusion coefficients and c_i is the intracellular volume fraction (Fig. 1). The extracellular volume fraction (c_e) was defined according to $c_i + c_e = 1$. For simplicity, $D = D_i = D_e$ was assumed in the present study.

In the one-dimensional Stejskal–Tanner pulsed gradient experiment investigated in this study, only the gradient amplitude g was varied in successive experiments while the direction $\mathbf{n}$ was fixed. Assuming rectangular gradient lobes with durations given by δ and the time between their leading edges given by Δ, Eq. (3) is rewritten as

$$\phi_k = \gamma g \mathbf{n} \cdot \left(\int_{t=0}^{\delta} \mathbf{r}_k(t) dt - \int_{t=\Delta}^{\Delta+\delta} \mathbf{r}_k(t) dt \right) = \gamma \delta g \mathbf{n} \cdot \Delta \mathbf{r}_k \tag{4}$$

where $\Delta\mathbf{r}_k$ is the difference between the centre-of-masses of the particle's trajectories during the two gradient lobes. Defining $\mathbf{q} = \gamma(2\pi)^{-1}\delta g\mathbf{n} = q\mathbf{n}$ and combining Eq. (2) with Eq. (4) gives

$$S^*(\mathbf{q}) = \sum_{k=1}^{n} \cos(2\pi \mathbf{q} \cdot \Delta \mathbf{r}_k) \tag{5}$$

Signal values for an arbitrary range of $\mathbf{q}$-values can be obtained from a single simulation where n samples $\Delta\mathbf{r}_k$ are drawn (simulated) from the $F(\Delta\mathbf{r})$ distribution, although this leads to correlated simulation noise in the signal-versus-q curve.

Discrete simulations were performed with $\mathbf{r}_k$ discretized in steps of Δx in space and in steps of $\Delta t(k) = \Delta x^2/2n_d D(k)$ in time, where n_d is the number of dimensions in the simulation (two or three) and $D(k)$ is the diffusion coefficient for the kth compartment. In each time increment, the particles were moved one step in a random direction. Note that care must be taken to ensure that the simulated gradient durations do not deviate from the specified values when the time is discretized.

Particles moving from an intracellular compartment i to the extracellular compartment e were only allowed to complete the transition with a probability $p(i,e)$, related to τ_i according to

$$p(i,e) = \left(\frac{n_{\text{tot}}}{n_{\text{out}}} \right)_i \cdot \frac{\Delta t(i)}{\tau_i} \tag{6}$$

where n_{tot} is the total number of possible displacements for particles inside compartment i and n_{out} is the number of displacements that would cause a transition out of compartment i during Δt [5]. If the transition was not fulfilled, the particles were elastically reflected back to their original positions, i.e. the membranes were considered to be positioned between the discrete points where the particles were positioned. In terms of membrane permeability (P), $p(i,e)$ is given by

$$p(i,e) = \frac{P\Delta x}{D(i)} = \frac{2n_d}{\Delta x} \frac{V}{A} \frac{\Delta t(i)}{\tau_i} \tag{7}$$

when assuming that $P = (1/\tau_i)\cdot(V/A)$, where V/A is the volume-to-surface fraction of the compartment and $n_d = 2$ [16]. When this assumption is valid, Eq. (7) is approximately equal to Eq. (6). For

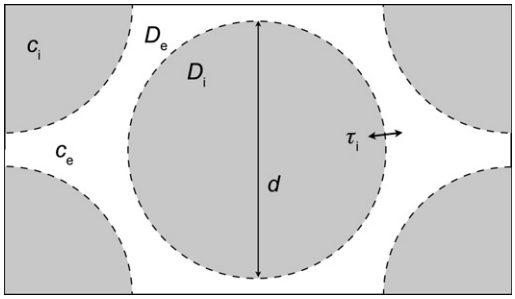

Fig. 1. The two-compartment simulation geometry (tissue model) investigated in the present study is described by the diameter d, the intra- and extracelular diffusion coefficients D_i and D_e, the intracellular volume fraction c_i (where $c_i + c_e = 1$) and the intracellular exchange time τ_i. In the present investigation, $D_i = D_e$ was assumed and thus four parameters described the simulation geometry. Note that ADC_e is estimated in the analytical model, which is related to D_e according to $ADC_e = D_e/\lambda^2$. The local patch illustrated in the figure was repeated infinitey, creating a hexagonal grid of simulated cells.

compartments without specified exchange times, such as the extracellular compartment, $p(e,i)$ was given by

$$p(e,i) = p(i,e)\frac{\Delta t(e)}{\Delta t(i)} \tag{8}$$

Note that this relationship assumes and implies identical particle concentrations in the different compartments.

The Monte Carlo formulation in Eq. (2) shows that S^* is the average of the stochastic variables $\cos(\phi)$. Therefore $V[S^*] = V[\cos(\phi)]/n^2$, with

$$\begin{aligned} V[\cos(\phi)] &= E[\cos^2(\phi)] - E[\cos(\phi)]^2 \\ &\approx \left(\frac{1}{n}\sum_{k=1}^{n}\cos^2(\phi_k)\right) - \left(\frac{1}{n}\sum_{k=1}^{n}\cos(\phi_k)\right)^2 \end{aligned} \tag{9}$$

where $E[\cdot]$ and $V[\cdot]$ are the expectation value and the variance of a stochastic variable, respectively [17]. In the asymptotic case where $q \to \infty$ and $S \to 0$, ϕ_k can be considered to be drawn from a uniform distribution on $[0,2\pi)$, where the variance is given by

$$V[\cos(\phi)] \approx \int_0^{2\pi}\cos^2(\phi)\frac{1}{2\pi}d\phi = \frac{1}{2} \tag{10}$$

In order to avoid too large an influence of the simulation noise on the estimated parameters when using a database of simulated signal curves to fit the measured signal curves, the condition $\sigma_s \ll \sigma_m$ should be fulfilled, where $\sigma_s = \sqrt{V[S^*]} \approx 1/2n$ and σ_m is the noise standard deviation in the measurements.

2.1. Analytical models

The employed analytical model was a two-compartment modified Kärger model, similar to models employed previously in various forms [5,7,10,13,18,19]. This model was defined using a matrix exponential according to

$$S(b) = S_0[\,1 \quad 1\,]\exp(-b\cdot\mathbf{ADC} + \mathbf{K}\cdot T_D)\begin{bmatrix} c_i \\ c_e \end{bmatrix} \tag{11}$$

where $b = (2\pi q)^2 T_D$ and T_D is the diffusion time $T_D = \Delta - \delta/3$ (infinitesimally short gradient ramp times assumed). The apparent diffusion coefficient matrix **ADC** is defined according to

$$\mathbf{ADC} = \begin{bmatrix} ADC_i & 0 \\ 0 & ADC_e \end{bmatrix} \tag{12}$$

with the intracellular ADC_i defined as

$$ADC_i = [d\cdot k(\alpha,\beta)]^2/2T_D \tag{13}$$

where $k(\alpha,\beta)$ is calculated using the gaussian phase distribution (GPD) approximation according to

$$k(\alpha,\beta) = \sqrt{\sum_{m=1}^{\infty}\frac{2\alpha a_m - 2 + 2\exp(-\alpha a_m) + \exp(-\beta a_m)\cdot(2-\exp(\alpha a_m) - \exp(-\alpha a_m))}{\alpha^2 a_m^3(a_m-1)}} \tag{14}$$

with a_m defined by $J'(\sqrt{a_m}) = 0$, so that $\sqrt{a_m}$ are the roots of the derivative of the Bessel function of the first kind and order one [20] and

$$\alpha = \frac{4\delta D_i}{d^2}, \quad \beta = \frac{4\Delta D_i}{d^2} \tag{15}$$

The extracellular ADC_e relates to D_e according to

$$ADC_e = D_e/\lambda^2 \tag{16}$$

where λ is the tortuosity factor of the extracellular space. The exchange matrix **K** was defined according to

$$\mathbf{K} = \begin{bmatrix} -k_{ie} & k_{ei} \\ k_{ie} & -k_{ei} \end{bmatrix} \tag{17}$$

where k_{ie} and k_{ei} are the exchange rates out of and into the intracellular compartment with $k_{ie}c_i = k_{ei}c_e$ and $k_{ie} = 1/\tau_i$.

This model utilizes six free parameters, $\mathbf{m} = \{S_0, d, \tau_i, ADC_e, D_i, c_i\}$, where S_0 is the signal without diffusion encoding and ADC_e is the apparent diffusion coefficient in the extracellular space.

3. Method

The simulation kernel for simulating $\Delta\mathbf{r}_k$ in Eq. (5) was implemented in C, and other programming was performed in MATLAB (MathWorks, Natick, MA). The simulations employed either a single thread on the central-processing unit (CPU), an Intel Core 2 Duo @ 2.13 GHz, or the GPU, a NVIDIA GeForce 9800 GT graphics card, supporting NVIDIA's compute unified device architecture (CUDA). The two versions were compared in a basic benchmark test of free diffusion, where the trajectories of $n = 107\,520$ particles were simulated during a simulation time period of 200 ms in steps of $\Delta t = 2.5$ μs. Random number generation was performed using the Multiply-With-Carry algorithm, in order to obtain high-quality random numbers in the parallel simulations on the GPU [21].

3.1. Validation of the simulation framework

The validity of the simulation framework was initially investigated by three categories of tests investigating free diffusion, restricted diffusion and compartmental exchange.

3.1.1. Free diffusion

Simulations of free diffusion were performed where signal-versus-b curves for b-values between 0 and 2500 s/mm^2 were generated for free diffusion with $\delta = 10$ ms and $T_D = 100$ ms ($\Delta x = \Delta y = 0.2$ μm, $D = 2.0$ μm^2/ms and $n = 2\times10^5$). The generated signal-versus-b curves was compared with the theoretical signal curves given by $S(b) = \exp(-bD)$, considering also the signal variance calculated according to Eq. (9).

3.1.2. Restricted diffusion

The effects of different step lengths Δx were investigated by simulated measurements performed perpendicular to a cylinder ($d = 10$ μm) using $\Delta x = \Delta y = d/60$, $d/45$, $d/30$ and $d/15$ μm, with $\delta \approx 0$ ms and $T_D = 500$ ms ($D = 1.0$ μm^2/ms, $n = 10^6$). Under these conditions, the intracellular signal-versus-q curve is expected to show a diffraction pattern according to the short gradient pulse approximation (SGP), given by

$$S(q) = \left(\frac{2J_1(\pi q d)}{\pi q d}\right)^2 \tag{18}$$

where J_1 is the Bessel function of the first kind [12]. To evaluate the effect of different step lengths, the diameter in Eq. (18) was estimated from the simulated signal-versus-q curves.

The effects of different diffusion encoding times δ on the signal curves were investigated by comparing signal curves from simulated measurements perpendicular to a cylinder, to those expected

from the GPD and SGP approximations in Eq. (13) and in Eq. (18), respectively. Two separate simulations were performed with $\delta = 15$ μs and $\delta = 15$ ms for $T_D = 500$ ms ($d = 10$ μm, $\Delta x = 0.2$ μm, $D = 2.0$ μm^2/ms, $n = 10^6$).

3.1.3. Compartmental exchange

The relation between τ_i and the probability of a membrane transition $p(i,e)$ in Eq. (6) was tested by simulations in a rectangular confinement using $n = 10^5$ intracellular particles for $\tau_i = 25$, 100 and 250 ms. The time that the kth particle spent in the intracellular compartment before its first membrane transition was recorded as $(T_i)_k$ and the effective exchange time $\hat{\tau}_i$ was estimated by fitting $n_i(t) = n\exp(-t/\hat{\tau}_i)$ to $\sum_{k=1}^{n} 1\{(T_i)_k < t\}$, where $1\{a < b\}$ equals unity if $a < b$ and zero otherwise [16]. This process was repeated 100 times and $\hat{\tau}_i$ was determined to be significantly longer than τ_i if more than 99% of the estimated $\hat{\tau}_i$ exceeded τ_i. This procedure was repeated for $\tau_i = 100$ ms using different step lengths, $\Delta x = d/60$, $d/45$, $d/30$ and $d/15$ μm, for diffusion perpendicular to a cylinder ($d = 10$ μm, $D = 2.0$ μm^2/ms, $n = 10^5$) and repeated 20 times to investigate the influence of simulation noise.

3.2. Evaluating diffusion MRI data

To investigate the accuracy and precision when estimating microstructural parameters from diffusion MRI data, a database with simulated signal-verus-b curves was constructed using 60 060 different combinations of microstructural tissue parameters $\mathbf{m} = \{d = 2, 3, \ldots, 14$ μm, $D = 1.0, 1.1, \ldots, 2.0$ μm^2/ms, $c_i = 25\%, 27.5\%, \ldots, 75\%$, $\tau_i = 50, 100, \ldots, 1000$ ms$\}$. The simulations were performed using $n = 107\,520$ particles and $\Delta x = d/40$ for $T_D = 30$ and 60 ms, with $\delta = 30$ ms. The signal-versus-b curve for each T_D was sampled by 41 different b-values linearly spaced between zero and 20 000 s/mm^2, corresponding to a maximal gradient strength of approximately 100 mT/m.

The microstructure parameters $\mathbf{m}$ were estimated for each combination $\mathbf{m}$ in the database, after adding noise to the simulated signal curves $\sigma_m = 0.025$, corresponding to $SNR = 40$ for $S(0)$. Simulated experiments were constructed by adding noise to the simulated signal curves according to $S_n = \sqrt{(S + N_r)^2 + N_i^2}$ where S_n is the noisy signal, S is the simulated signal and N_r and N_i are gaussian noise with mean zero and standard deviation σ_m.

The model parameters were estimated by fitting the models to the simulated experiment, by finding the signal curves in the database that produced the least squared difference to the simulated experiment, including only signal values exceeding $3\sigma_m$. For this purpose, a database of analytical signal-versus-b curves was constructed for the same microstructural parameters as in the database of simulated signal curves. Since the simulation model contained only four free parameters, two of the six parameters in the analytical model were fixed to their true values, i.e. S_0 and D_i, in order to allow fair comparisons of the models. Moreover, specific simulations with impermeable membranes and particles only in the extracellular space were performed to estimate λ in Eq. (16), in order to determine the expected value of ADC_e. The estimated value of λ was obtained as the average value of the simulations performed with $T_D = 30$ and 60 ms.

The distributions of the fitted parameters, obtained from fitting the models to 1000 different simulated experiments, were initially investigated for two different sets of microstructural parameters $\mathbf{m}$. The accuracy and precision in the estimated parameters were then investigated by studying the bias and the coefficient of variation (CV) of the estimated parameters. The bias was defined as mean $(\hat{\theta})/\theta - 1$, where θ is the true value of the parameter of interest and mean$(\hat{\theta})$ is the mean value of that parameter estimate. The CV was defined as $\sigma(\hat{\theta})/\theta$, where $\sigma(\hat{\theta})$ is the standard deviation of the parameter estimate. The bias and the CV were estimated for all combinations of microstructural parameters with $D = 1.7$ μm^2/ms, by fitting the models to 50 different simulated experiments for each combination of microstructural parameters.

As discrepancies between the signal curves obtained with the analytical model and the simulation model were found, simulations were carried out using another simulation kernel constructed to fulfill the assumptions of the analytical model. Diffusion in two freely diffusing water pools was simulated, where the ADC values of the two water pools were $ADC_e = D/\lambda^2$, with $D = 1.7$ μm^2/ms and $\lambda = 1.32$ and ADC_i as obtained from Eq. (13) with $d = 10$ μm. The probability of the particles to change water pools was constant at $p_0(i,e) = \Delta t/\tau_i$ and $p_0(e,i) = p_0(i,e)\cdot c_i/c_e$, with $\tau_i = 50$ ms and $n = 2 \times 10^5$ particles were simulated using the same protocol as in the other simulations. Note that these simulation were physically unrealistic.

4. Results

4.1. Validation of the simulation framework

The parallel GPU simulations were approximately 26 times faster than simulations on the CPU (238 s versus 9.3 s). Subsequent simulations were therefore performed using the GPU.

4.1.1. Free diffusion

The simulated signal-versus-b curve was within the 95% confidence level of the theoretical signal curve for free diffusion (Fig. 2).

4.1.2. Restricted diffusion

When Δx was varied between $d/60$ and $d/15$ ($d = 10$ μm), the estimated cylinder diameter deviated less than 0.3% from the true value. Diffraction patterns in the signal-versus-q curves were clearly observed in the simulated signal-versus-q curves when $\alpha \to 0$ and $\beta = 40$ (Fig. 3), expected according to the SGP approximation for measurements performed perpendicular to a cylinder. In the second case, where the SGP approximation was violated ($\alpha = 1.2$), the simulated signal curve and the curve from the GPD approximation agreed well for a signal attenuation up to approximately one magnitude. At larger signal attenuations, the GPD approximation is not valid (Fig. 3b).

4.1.3. Compartmental exchange

The validity of Eq. (6) was investigated for three different intracellular exchange times $\tau_i = 25$, 100 and 250 ms. The

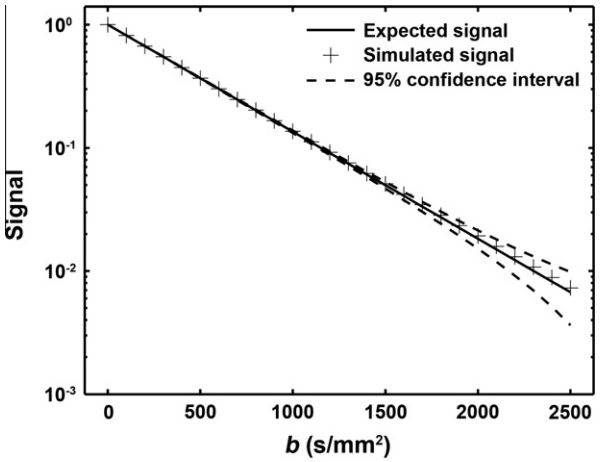

Fig. 2. Signal-versus-b curve with 95% confidence interval, obtained from a simulation of free diffusion ($D = 2.0$ μm^2/ms) using $n = 2 \times 10^5$ particles. This result indicates a correct implementation of the diffusion encoding.

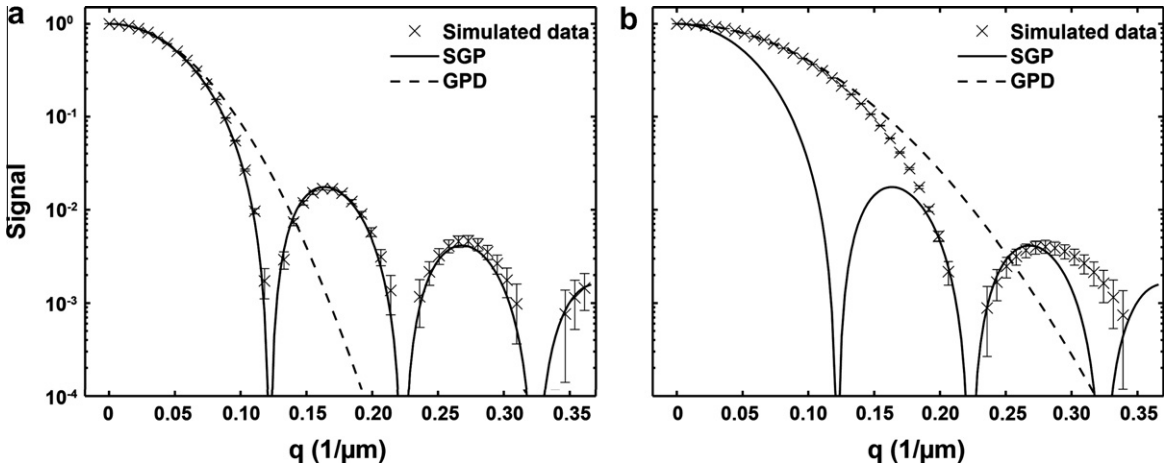

Fig. 3. Signal-versus-q curves from a simulated measurement perpendicular to a cylinder (d = 10 μm), with all particles confined inside a cylinder. (a) When α was virtually zero (δ = 15 μs), the SGP approximation was valid and the simulated signal curve showed the expected diffraction pattern. (b) For α = 1.2 (δ = 15 ms), the simulated signal curve and the curve from the GPD approximation agreed well for a signal attenuation less than approximately one magnitude.

estimated values were $\hat{\tau}_i = 27.0 \pm 0.17$ ms, 102 ± 0.65 ms and 252 ± 1.6 ms (mean ± one standard deviation), see Fig. 4a. The estimated values were significantly longer than the expected values for τ_i = 25 and 100 ms. As Δx was varied, the estimated values varied only minimally:

$\hat{\tau}_i = 101.46 \pm 0.37,$
$101.25 \pm 0.41,$
$101.41 \pm 0.52,$
101.72 ± 0.46 ms

for $\Delta x = d/15$, $d/30$, $d/45$ and $d/60$, respectively. Note that the particle distribution within the compartment became non-uniform as the simulation elapsed (Fig. 4b).

4.2. Evaluating diffusion MRI data

The distributions of the estimated model parameters **m**, obtained using the simulation and the analytical model, are shown in Fig. 5 for two examples with different sets of microstructural parameters. The estimated distributions overlapped to a large extent for τ_i, but differed for most of the other parameters. For example, the analytical model overestimated the diameter in the case where d = 3 μm, in contrast to the simulation model. The difference in D between the analytical and the simulation model is a matter of definitions, since D in the analytical model corresponds to ADC_e, while for the simulations, it refers to the diffusion coefficient of all water ($D = D_i = D_e$). However, the estimated values of ADC_e were close their the expected values, as calculated from Eq. (16), with λ estimated from a simulation with extracellular particles only in an identical geometry, but with impermeable membranes. For c_i, both models produced the close to the correct estimate for the higher c_i with longer τ_i, while c_i was underestimated in the example with short τ_i when using analytical model.

The distributions of the estimated parameters were characterised by their bias and coefficient of variation for all sets of model parameters **m** with D = 1.7 μm^2/ms and $c_i \geqslant 50\%$. For the analytical model, the reference value of ADC_e was set according to Eq. (16) with λ estimated from the specific simulations with extracellular particles only. The obtained values of λ, when averaged over all included entries in the database, was 1.35 ± 0.06 (mean ± one standard deviation). The bias and the CVs were averaged over all investigated c_i and the resulting maps are shown in Figs. 6 and 7, respectively.

Using the analytical Kärger model, the bias in d was lower than 10% when $d \geqslant 4$ μm and $\tau_i \geqslant 500$ ms, but for τ_i = 100 ms, the bias was low only when $d \geqslant 8$ μm. Exchange times were accurately estimated (bias $\leqslant$10%) for $\tau_i \leqslant 900$ ms and $d \leqslant 9$ μm, but generally showed large biases otherwise. The intracellular volume fraction c_i

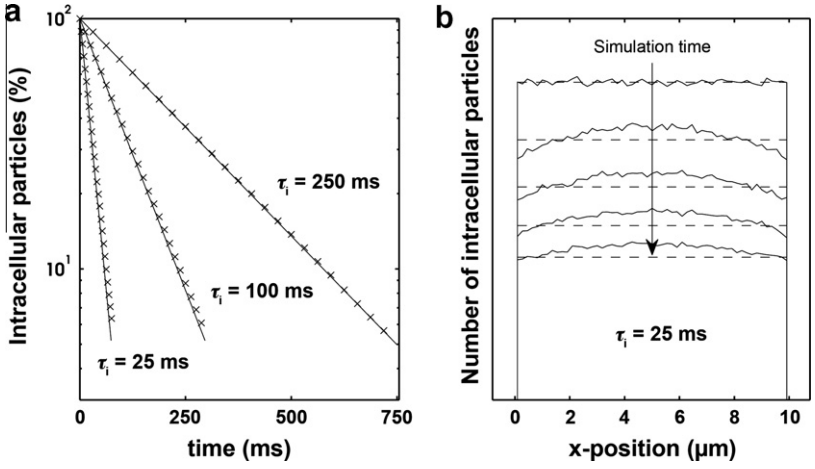

Fig. 4. (a) The percentage of particles that never passed the membrane, i.e. remained intracellular as the simulation time elapsed. Solid lines indicate the expected curve and the crosses show the results from the simulations. (b) The distribution of particles within the rectangular confinement became non-uniform as the time elapsed. The solid line shows the simulated distribution of intracellular particles and the dashed line the uniform distribution assumed in the Kärger model.

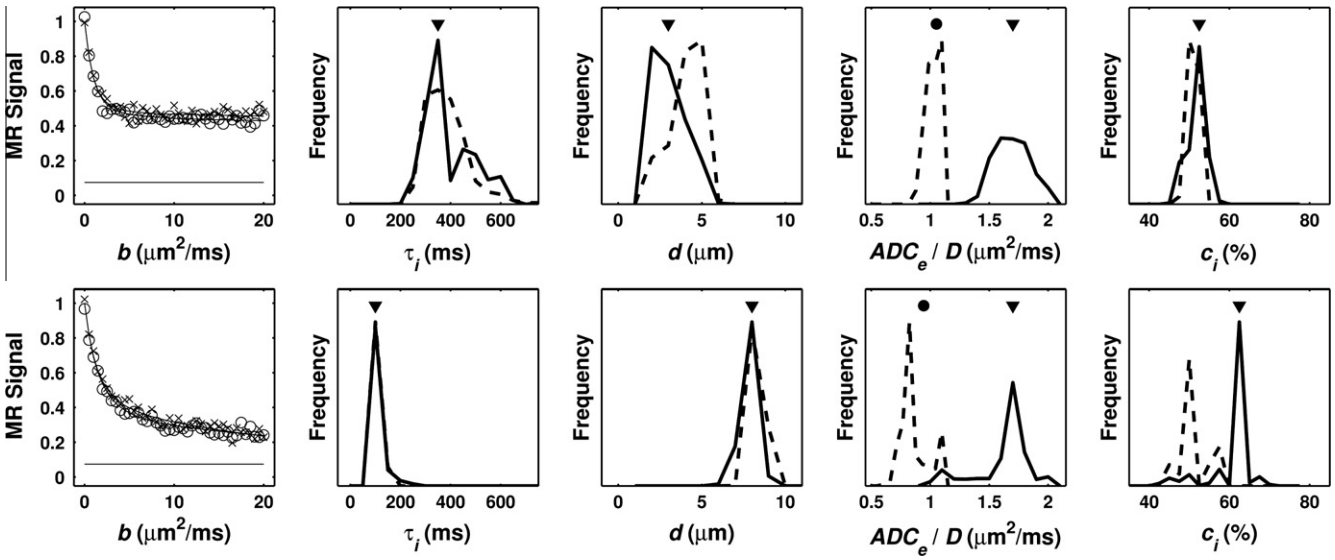

Fig. 5. Simulated signal-versus-b curves for T_D = 30 ms (circles) and T_D = 60 ms (crosses), shown in the leftmost column for two different examples in the top and bottom rows, respectively. The solid horizontal black line corresponds to $3\sigma_m$, below which no signal values were included in the fitting. The distributions of the estimated parameters τ_i, d, ADC_e or D and c_i are shown from left to right, estimated using the analytical model (dashed line) and the simulation model (solid line) from 1000 different simulated experiments. The estimated diffusion coefficients represent ADC_e in the analytical model and $D = D_i = D_e$ in the simulation model. The true values are indicated by black triangles, but for ADC_e it is indicated by a black circle. Note that c_i was underestimated when using the analytical model in the second example.

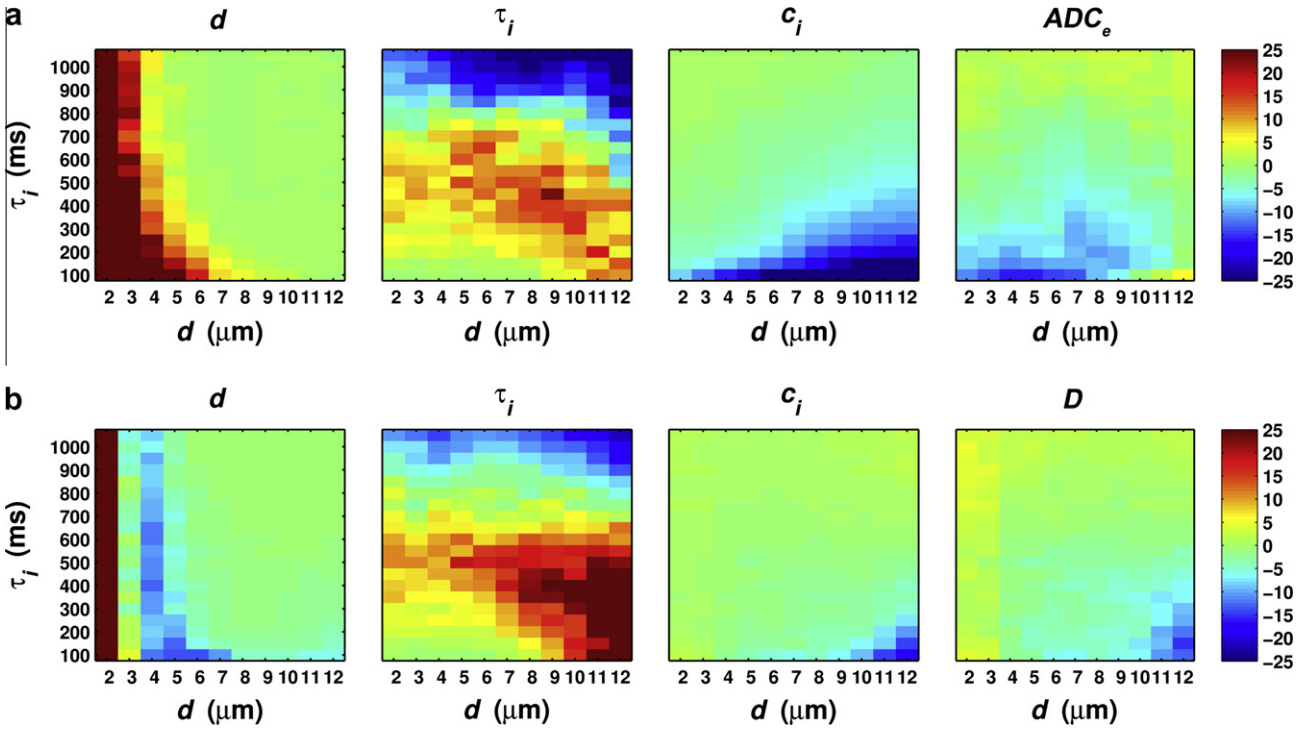

Fig. 6. The bias in percent of the true value is shown for the analytical model (a) and the simulation model (b). The x- and y-scales represent d and τ_i, respectively. Only results simulated with D_i = 1.7 μm²/ms and the bias values were averaged for $c_i \geqslant 50\%$. The true values of ADC_e in the analytical model were calculated using Eq. (16) with λ obtained from dedicated simulations with extracellular particles only and impermeable membranes.

was negatively biased for short exchange times ($\tau_i \leqslant 200$ ms) and larger diameters ($d \geqslant 5$ μm) and the bias in ADC_e was generally low. Using the simulation model, the biases in the estimated parameters were generally similar to those obtained when using the analytical model. The bias in d was for small diameters negative as opposed to positive for the analytical model, while the bias for τ_i was slightly higher. Notably, the bias in c_i found for the analytical model nearly vanished when using the simulation model.

The coefficients of variation were nearly identical for the analytical model and the simulation model. The CVs in d were below 10%, when $d \geqslant 4$–5 μm, but up to 50% for smaller d. The lowest CVs, generally below 10%, was found for c_i. In τ_i, the CVs were low only for $\tau_i \leqslant 200$ ms, but were otherwise as high as 40%.

Signal-versus-b curves from the compartment simulations were compared with the simulations of two freely diffusing water pools with a constant probability of exchange. The obtained results were

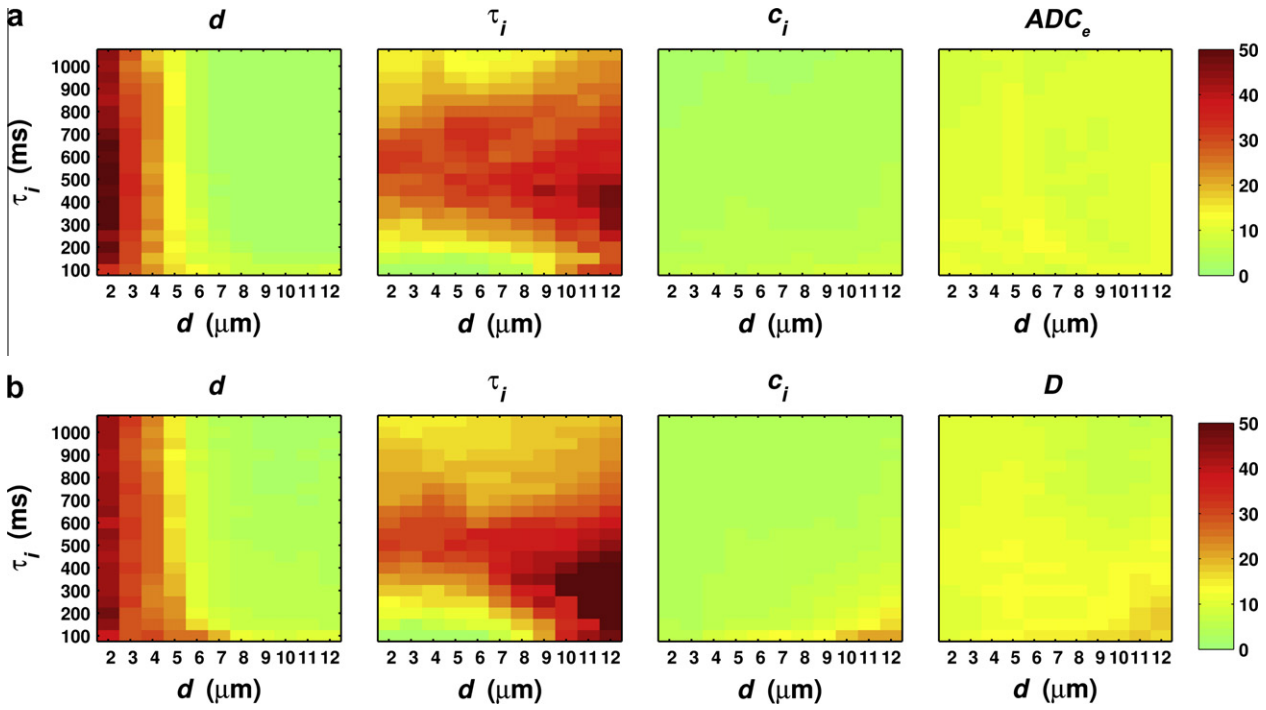

Fig. 7. The coefficient of variation is shown for the analytical model (a) and the simulation model (b). The x-and y-scales represent d and τ_i, respectively. Only results simulated with $D_i = 1.7$ μm^2/ms are shown and the values of CV were averaged for $c_i \geqslant 50\%$.

highly different (Fig. 8). For the compartment simulations, where exchange only occurs after a successful membrane transition, a bias was induced in the parameters estimated by the analytical model (Fig. 8a). For the simulations performed with a constant probability of exchange between the water pools, the model returned almost the correct values since those simulations fulfilled the assumptions in the analytical model (Fig. 8b).

5. Discussion

Signal-versus-*b* curves in nerve tissue are known to be non-monoexponential, i.e. reflecting multiple water pools with different *ADC* values [19]. These pools are assumed to origin from one extracellular component and one or several intracellular components showing restricted diffusion [5,6,10,11,22]. If the compartments are assumed to be in the slow exchange regime, with negligible exchange occurring during the diffusion time, the bias in the estimated d is small for $d \geqslant 5$ μm, when an measurement protocol optimized for a clinical MRI scanner is employed [6]. Water exchange between compartments might, however, influence high *b*-value diffusion measurements in fixated nervous tissue as well as *in vivo* [5,10,23]. The modified Kärger equations employed in Eq. (11) allows for exchange to be included in analytical diffusion models [5,10], but the equations assume a constant probability over time for a compartment exchange [18]. This assumption is not valid for diffusion restricted in a compartment (Fig. 4b). As a result, the estimated parameters are biased when using the analytical measurement model (Fig. 6a). However, the parameters are in some cases biased also when using the simulation model (Fig. 6b), due to measurement noise in combination with limitations in the measurement protocol. For example, prolonging T_D would most likely reduce the bias in τ_i, for both models.

A resolution limit of approximately 4 μm was observed under slow exchange conditions, similar to the results presented by

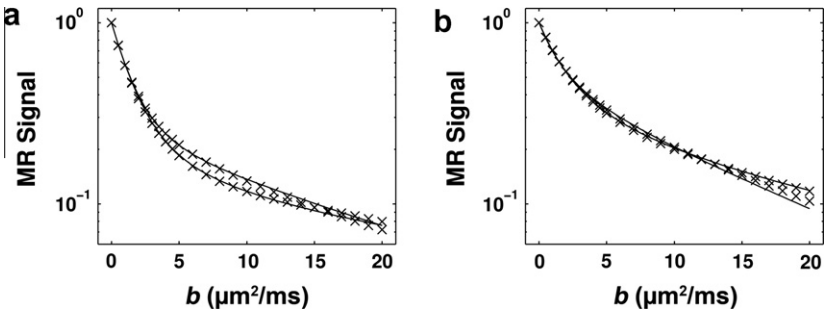

Fig. 8. The plots show signal-versus-*b* curves simulated in two different compartments using $d = 10$ μm, $D = 1.7$ μm, $c_i = 60\%$ and $\tau_i = 50$ ms (a) and in a specially designed simulation of water diffusing freely in two different water pools (b). In the specially designed simulation, the probability of exchange between the water pools was constant and the *ADC* values in the different pools were selected to match those defined by the analytical model for the microstructural parameters investigated in (a). The solid line represents the best fit of the analytical model, where the estimated parameters were (a) $c_i = 35\%$, $ADC_e = 0.88$ μm^2/ms, $d = 10$ μm and $\tau_i = 50$ ms for the compartment simulation and (b) $c_i = 65\%$, $ADC_e = 1.1$ μm^2/ms, $d = 11$ μm and $\tau_i = 50$ ms for the water pool simulation. This shows that the analytical model underestimates c_i from the compartment simulation, while it returns almost the correct value for the (unphysical) simulation specially designed to fulfill the assumptions of the analytical model.

Alexander [6]. The cause of the bias in d is the extremely low signal attenuation of the intracellular signal, due to the nearly zero ADC_i for d smaller than the resolution limit. An increase in the maximal gradient strength could lower the resolution limit by allowing shorter δ. Improving the resolution limit from d_1 to $d_2 = d_1/2$ could be expressed as the condition $b_1 \cdot ADC_i(d_1, \alpha_1, \beta_1) = b_2 \cdot ADC_i(d_2, \alpha_2, \beta_2)$, i.e. that the intracellular signal attenuation should be equally large at the smaller d. This condition holds if $b_2 = b_1$, $\alpha_2 = \alpha_1$ and $\beta_2 = \beta_1$, which requires $\delta_2 = \delta_1/4$ as well as $(T_D)_2 = 1/4 \cdot (T_D)_1$. In order to fulfill $b_2 = b_1$, the maximal gradient amplitude must increase eightfold, i.e. $g_2 = 8g_1$. This result was described by Lätt et al. in the context of q-space diffusion MRI [24].

The observed bias in c_i when using the analytical model under fast exchange conditions (Fig. 6a) might hamper interpretation of diffusion measurements. For example, Clark et al. observed a slow diffusion fraction smaller than expected if that fraction originated from intracellular water and concluded that this mismatch might be caused by a rapid exchange. Indeed, generating biexponential and diffusion time independent signal-versus-b curves using the parameters for gray matter presented by Clark et al. ($c_{\text{fast/slow}}$ = 71/29% and $ADC_{\text{fast/slow}}$ = 1.02/0.19 μm^2/ms) and evaluating data using the simulation model yields $c_i = 51 \pm 7\%$, $d = 12 \pm 1.6$ μm, $\tau_i = 61 \pm 22$ ms, using $SNR = 40$ and assuming $D = 1.7$ μm^2/ms. The value of c_i is still lower than the expected value of 80%, but warrants further investigations.

One limitation of the present study was that possible parameter bias in relation to the true tissue-related parameters caused, for example, by an oversimplified tissue model was not evaluated. Moreover, the measurement protocol chosen in the present study represent a high b-value protocol with sequence parameters obtainable with a clinical MRI scanner. The protocol might be optimized for improved accuracy of certain parameters [6]. However, we recommend the presently described methods for detecting biases to be employed before interpreting results obtained with protocols other than the one examined in this study. The simulations and the subsequent data evaluations require a computation time of approximately a week on a desktop computer.

Another limitation was that the simulation model used the same model to generate data as for estimating the parameters, in contrast to the analytical model. This could have resulted in slightly higher biases and coefficients of variation for the analytical model, although the negative bias in c_i for short τ_i clearly originated from the assumptions in the analytical model (Fig. 8). The results were also influenced by the reduction of two parameters in the analytical model. For example, instead of fixing D_i, it could have been included in the fitting with ADC_e calculated according to Eq. (16), knowing that $D_e = D_i$ and with λ estimated in separate simulations. This was approach was not chosen since any deviation in D would have resulted in a deviation also in d, since these parameters are related via Eq. (13). Simulation noise, although much smaller in amplitude than the applied measurement noise, likely had a marginal influence on results from single simulations (Fig. 5). The bias and coefficient of variations maps, however, were averaged over simulations performed with different c_i, resulting in less influence on the results from the simulation noise. At higher SNR of the simulated experiment, the correlated simulation noise would have a larger influence.

Fast simulations were required in order to allow a large number of simulations to be performed with different microstructural parameters in a short time. This was achieved by performing parallel simulations on a discrete simulation grid using a modern GPU. Continuous particle displacements, as employed in some studies [13,25,26], may seem more realistic than discrete displacements, but other studies have confirmed that discrete simulations are feasible and of acceptable quality [15,27,31]. Discrete step sizes are also more efficient from a numerical perspective [31]. Simulations with discrete steps in all directions, as employed in the present framework, do not require the handling of multiple membrane reflections, as discussed by Hall and Alexander [31]. However, in order to allow the fractions of intra- and extracellular space to be sufficiently well specified, our design enforced shorter step lengths than required when using continuous displacements. This was a disadvantage of the present simulation framework, since longer step lengths are generally more computationally efficient [31].

The quality tests ensured that the simulation framework generated reliable results. The simulated signal curves in case of free and restricted diffusion were in agreement with the theoretically predicted results, independently of the step length within a reasonable interval (Figs. 2 and 3). However, the estimated effective exchange times were slightly longer than expected for all investigated step sizes (Fig. 4). This small bias was caused by the definition of τ_i in the derivation of Eq. (6), since for high exchange probabilities, the concentration of particles that had never experienced a membrane transition became non-uniform as the time elapsed (Fig. 4b), thereby violating the requirements for Eq. (6) [5]. Nevertheless, this minimal bias can be neglected when $\tau_i \geqslant 50$ ms.

The present investigation was based on the Stejskal–Tanner pulse sequence, but other gradient waveforms are easily simulated by modifying the assumed gradient waveform, for example, to simulate double-wave vector diffusion MRI [28,29]. Another advantage of using simulations as the measurement model is that it allows the use of complex geometries as the tissue model. Available analytical models for the intracellular signal curves only allows simple geometries, such as planes, cylinders and spheres as the tissue model. Similarly, the extracellular space is commonly modelled as a mono-exponential signal-verus-b curve, although it is plausible that it is non- mono-exponential for intermediate diffusion times [30]. These issues are extraneous when using simulations as the measurement model, since the signal curves are implicitly given by the simulation geometry.

In conclusion, signal-versus-b curves simulated for conditions and noise levels achievable on a clinical MRI scanner were evaluated using an analytical two-compartment model as well as by matching them with signal curves produced by Monte Carlo simulations, i.e. the simulation model. Both models produced a bias in the estimated diameter for diameters smaller than approximately 4 μm. A major negative bias was found in the intracellular volume fraction for exchange times shorter than approximately 350 ms when using the analytical model. This bias nearly vanished when using the simulation model. This work could potentially improve the possibility of absolute quantification of tissue microstructural properties using diffusion MRI. The simulation framework and the required source code for this analysis are available on request as open-source software.

Acknowledgments

The authors are grateful to Prof. Elisabet Englund for helpful discussions. This study was supported by the Swedish Cancer Society (Grant no. CAN 2006/1272), the Swedish Research Council (Grant no. 13514), the Crafoord Foundation Lund and the Lund University Hospital Donation Funds.

References

[1] Y. Assaf, Y. Cohen, Assignment of the water slow-diffusing component in the central nervous system using q-space diffusion MRS: implications for fiber tract imaging, Magn. Reson. Med. 43 (2) (2000) 191–199.
[2] Y. Cohen, Y. Assaf, High b-value q-space analyzed diffusion-weighted MRS and MRI in neuronal tissues – a technical review, NMR Biomed. 15 (7–8) (2002) 516–542.

[3] Y. Assaf, T. Blumenfeld-Katzir, Y. Yovel, P.J. Basser, AxCaliber: a method for measuring axon diameter distribution from diffusion MRI, Magn. Reson. Med. 59 (6) (2008) 1347–1354.
[4] J. Lätt, M. Nilsson, A. Rydhög, R. Wirestam, F. Ståhlberg, S. Brockstedt, Effects of restricted diffusion in a biological phantom: a q-space diffusion MRI study of asparagus stems at a 3T clinical scanner, Magn. Reson. Mater. Phys. Biol. Med. 20 (4) (2007) 213–222.
[5] M. Nilsson, J. Lätt, E. Nordh, R. Wirestam, F. Ståhlberg, S. Brockstedt, On the effects of a varied diffusion time in vivo: is the diffusion in white matter restricted?, Magn Reson. Imaging 27 (2) (2009) 176–187.
[6] D.C. Alexander, A general framework for experiment design in diffusion MRI and its application in measuring direct tissue-microstructure features, Magn. Reson. Med. 60 (2) (2008) 439–448.
[7] J. Lätt, M. Nilsson, D. van Westen, R. Wirestam, F. Ståhlberg, S. Brockstedt, Diffusion-weighted MRI measurements on stroke patients reveal water-exchange mechanisms in sub-acute ischaemic lesions, NMR Biomed. 22 (6) (2009) 619–628.
[8] D. Barazany, P. Basser, Y. Assaf, In-vivo measurement of the axon diameter distribution in the rat's corpus callosum, in: Proceedings 16th Scientific Meeting, International Society for Magnetic Resonance in Medicine, Toronto, 2008, p. 567.
[9] P.N. Sen, Time-dependent diffusion coefficient as a probe of geometry, Concepts Magn. Reson. A 23 (1) (2004) 1–21.
[10] G.J. Stanisz, A. Szafer, G.A. Wright, R.M. Henkelman, An analytical model of restricted diffusion in bovine optic nerve, Magn. Reson. Med. 37 (1) (1997) 103–111.
[11] Y. Assaf, P.J. Basser, Composite hindered and restricted model of diffusion (charmed) MR imaging of the human brain, Neuroimage 27 (1) (2005) 48–58.
[12] W.S. Price, Pulsed-field gradient nuclear magnetic resonance as a tool for studying translational diffusion: Part 1. Basic theory, Concepts Magn. Reson. 9 (5) (1997) 299–336.
[13] C. Meier, W. Dreher, D. Leibfritz, Diffusion in compartmental systems i a comparison of an analytical model with simulations, Magn. Reson. Med. 50 (3) (2003) 500–509.
[14] J. van den Enden, D. Waddington, H. van Aalst, van Kralingen CG, K. Packer, Rapid determination of water droplet size distributions by PFG-NMR, J. Colloid Interface Sci. 140 (1) (1990) 105–113.
[15] P. Linse, O. Söderman, The validity of the short-gradient-pulse approximation in NMR studies of restricted diffusion simulations of molecules diffusing between planes in cylinders and spheres, J. Magn. Reson. A 116 (1) (1995) 77–86.
[16] D. Regan, P. Kuchel, Mean residence time of molecules diffusing in a cell bounded by a semi-permeable membrane: Monte Carlo simulations and an expression relating membrane transition probability to permeability, Eur. Biophys. J. 29 (2000) 221–227.
[17] B. Lindgren, Statistical Theory, Chapman & Hall, New York, 1993.
[18] J. Kärger, Der einfluß der zweibereichdiffusion auf die spinechodämpfung unter berücksichtigung der relaxation bei messungen mit der methode der gepulsten feldgradienten, Anna Physik 482 (1) (1971) 107–109.
[19] T. Niendorf, R.M. Dijkhuizen, D.G. Norris, M. van Lookeren Campagne, K. Nicolay, Biexponential diffusion attenuation in various states of brain tissue: implications for diffusion-weighted imaging, Magn. Reson. Med. 36 (6) (1996) 847–857.
[20] P. van Gelderen, D. DesPres, P.C. van Zijl, C.T. Moonen, Evaluation of restricted diffusion in cylinders: phosphocreatine in rabbit leg muscle, J. Magn. Reson. B 103 (3) (1994) 255–260.
[21] G. Marsaglia, Random number generators, J. Mod. Appl. Stat. Methods 2 (1) (2003) 2–13.
[22] A. Szafer, J. Zhong, A.W. Anderson, J.C. Gore, Diffusion-weighted imaging in tissues: theoretical models, NMR Biomed. 8 (7–8) (1995) 289–296.
[23] C.A. Clark, D. Le Bihan, Water diffusion compartmentation and anisotropy at high b values in the human brain, Magn. Reson. Med. 44 (6) (2000) 852–859.
[24] J. Lätt, M. Nilsson, C. Malmborg, H. Rosquist, R. Wirestam, F. Ståhlberg, D. Topgaard, S. Brockstedt, Accuracy of q-space related parameters in MRI: simulations and phantom measurements, IEEE Trans. Med. Imaging 26 (11) (2007) 1437–1447.
[25] S. Peled, New perspectives on the sources of white matter DTI signal, IEEE Trans. Med. Imaging 26 (11) (2007) 1448–1455.
[26] G.T. Balls, L.R. Frank, A simulation environment for diffusion weighted MR experiments in complex media, Magn. Reson. Med. 62 (3) (2009) 771–778.
[27] B. Balinov, B. Jönsson, P. Linse, O. Söderman, The NMR self-diffusion method applied to restricted diffusion simulation of echo attenuation from molecules in spheres and between planes, J. Magn. Reson. A 104 (1) (1993) 17–25.
[28] M.A. Koch, J. Finsterbusch, Compartment size estimation with double wave vector diffusion-weighted imaging, Magn. Reson. Med. 60 (1) (2008) 90–101.
[29] M.E. Komlosh, F. Horkay, R.Z. Freidlin, U. Nevo, Y. Assaf, P.J. Basser, Detection of microscopic anisotropy in gray matter and in a novel tissue phantom using double pulsed gradient spin echo MR, J. Magn. Reson. 189 (1) (2007) 38–45.
[30] E. Fieremans, Y. De Deene, S. Delputte, M.S. Ozdemir, Y. D'Asseler, J. Vlassenbroeck, K. Deblaere, E. Achten, I. Lemahieu, Simulation and experimental verification of the diffusion in an anisotropic fiber phantom, J. Magn. Reson. 190 (2) (2008) 189–199.
[31] M.G. Hall, D.C. Alexander, Convergence and parameter choice for Monte-Carlo simulations of diffusion MRI, IEEE Trans. Med. Imaging 9 (2009) 1354–1364.